Title	Hybrid functional study of nonlinear elasticity and internal strain in zinc-blende III-V materials
Author(s)	Tanner, Daniel S. P.; Caro, Miguel A.; Schulz, Stefan; O'Reilly, Eoin P.
Publication date	2019-01-10
Original citation	Tanner, D.S., Caro, M.A., Schulz, S. and O'Reilly, E.P., 2019. Hybrid functional study of nonlinear elasticity and internal strain in zinc-blende III-V materials. Physical Review Materials, 3(1), (013604). DOI:10.1103/PhysRevMaterials.3.013604
Type of publication	Article (peer-reviewed)
Link to publisher's version	https://journals.aps.org/prmaterials/abstract/10.1103/PhysRevMaterials.3.013604 http://dx.doi.org/10.1103/PhysRevMaterials.3.013604 Access to the full text of the published version may require a subscription.
Rights	© 2019 American Physical Society
Item downloaded from	http://hdl.handle.net/10468/9072

Hybrid functional study of nonlinear elasticity and internal strain in zinc-blende III-V materials

Daniel S. P. Tanner,[1,*] Miguel A. Caro,[2,3] Stefan Schulz,[1] and Eoin P. O'Reilly[1,4]

[1]*Tyndall National Institute, Lee Maltings, Dyke Parade, Cork T12 R5CP, Ireland*
[2]*Department of Electrical Engineering and Automation, Aalto University, Espoo 02150, Finland*
[3]*Department of Applied Physics, Aalto University, Espoo 02150, Finland*
[4]*Department of Physics, University College Cork, Cork T12 YN60, Ireland*

We investigate the elastic properties of selected zinc-blende III-V semiconductors. Using hybrid functional density functional theory, we calculate the second- and third-order elastic constants and first- and second-order internal strain tensor components for Ga, In, and Al containing III-V compounds. For many of these parameters, there are no available experimental measurements, and this work is the first to predict their values. The stricter convergence criteria for the calculation of higher-order elastic constants are demonstrated, and arguments are made based on this for extracting these constants via the calculated stresses, rather than the energies, in the context of plane-wave-based calculations. The calculated elastic properties are used to determine the strain regime at which higher-order elasticity becomes important by comparing the stresses predicted by a lower- and a higher-order elasticity theory. Finally, the results are compared with available experimental literature data and previous theory.

I. INTRODUCTION

Elastic constants are fundamental material parameters, a knowledge of which is essential for the design and understanding of semiconductor materials and devices. For example, the electronic and optical properties of semiconductor heterostructures are strongly influenced by the strain state of their active regions [1]. This strain state depends on the lattice mismatch between the constituent compounds, and on the relative magnitude of their elastic constants [2]. Elastic constants are also necessary for the determination of the material composition of heterostructures by x-ray diffraction [3], assessing the critical thickness and strain relaxation in devices [4], modeling the behavior of dislocations [5], the characterisation of piezoelectric resonators [6], and the parametrization of interatomic potentials [7] used for the calculation of strain fields in supercells containing millions of atoms.

For crystals that lack inversion symmetry, standard macroscopic elasticity theory does not fully describe the position of their atoms under strain, and *internal strain* [8–10] occurs. Internal strain is a displacement between sublattices in a crystal. It is described, for a particular material, by the components of the internal strain tensor. Knowledge of these material parameters is essential for any semiempirical atomistic modeling which requires the equilibrium atomic positions of strained structures, and has, for instance, particular importance for the piezoelectricity of a crystal [11,12].

For many device and material applications, infinitesimal strain theory [13], in which there appear only second-order elastic constants (SOEC) and first-order internal strains, is sufficient to describe the elastic properties. This means that

the crystal energy can be accurately expressed to second order in the strain, with the SOECs as coefficients, and that the internal strain can be described accurately to first order in the strain, with the first-order internal strain tensor components (ISTCs) as coefficients. However, as the strain in the system increases, its energy (internal strain) can no longer be accurately described using only a second (first)-order expansion in the strain, and higher-order terms need to be accounted for. The lowest-order of such corrections are third-order elastic constants (TOEC) for the macroscopic strain energy, and second-order ISTCs for the internal strain. The strain magnitudes at which these corrections to the energy and internal relaxation become important will depend on the relative magnitudes of the higher- and lower-order coefficients of the strains.

Recent studies have shown that third-order contributions to the elastic energy are necessary to correctly model the relaxation, strain state, and thus optical properties, of several technologically important heterostructures such as InGaAs/GaAs [14–18], InGaN/GaN, and GaN/AlGaN [18–22]. Similar effects can be expected in other highly lattice-mismatched nanostructured systems, such as the InSb/GaSb quantum dot (QD) system [23]. Furthermore, second-order ISTCs have been shown to play an important role in the piezoelectric response in many materials [24,25]. Other phenomena related to lattice anharmonicity, such as phonon-phonon or electron-phonon interactions [26], thermal expansion [26], stress or temperature dependent elastic response [26], and pressure dependence of optic mode frequencies [27], also require the use of TOECs and second-order ISTCs.

Because of this wide application, there has long been interest in the measurement or theoretical determination of TOECs [28–31]. Typically, TOECs are measured using the velocity of sound waves through a crystal under uniaxial or

hydrostatic stress [32], analyzed via the finite strain theory of Murnaghan [33,34]. However, there are often very large uncertainties in such measurements [35], and these difficulties are compounded for brittle or metastable semiconductor materials [27,36,37], which are often of interest for device applications. Similarly, for the *internal* strain, of the materials addressed in this paper, only GaAs and InSb have available experimental values of their single first order ISTC (Kleinman parameter), due to the high precision of experimental observations required [27,38] for the extraction of ISTCs; there are no experimental evaluations of any second-order ISTCs. Thus, given the experimental difficulty in the measurement of ISTCs in general and the importance of nonlinear elasticity for the accurate description of the electronic and optical properties of technologically relevant semiconductors and their connected heterostructures, there is strong motivation for the theoretical determination of TOECs and first- and second-order ISTCs.

Early calculations of TOECs involved the use of pseudopotential [39] and interatomic force potential methods [29]; however, since the work of Nielsen and Martin [40], first-principles calculations have become an increasingly popular route towards the calculation of TOECs. In recent years, *ab initio* methods have been used to determine the TOECs for ultrahard materials such as diamond [41,42], materials of which it is difficult to obtain high quality single crystals, like the metastable cubic-phase nitride materials [19], and technologically important materials for which experimental TOEC measurements are sparse, such as InAs and GaAs [18,19,40,43].

In this work, we present first-principles calculations of SOECs, TOECs, as well as first and second-order ISTCs, of a range of III-V zinc-blende (ZB) semiconductor compounds. The calculations are carried out using density functional theory (DFT) within the Heyd-Scuseria-Ernzerhof (HSE) hybrid-functional approach [44]. We demonstrate that higher-order elastic properties require a higher resolution of calculation parameters for their accurate evaluation, and extend arguments present in the literature for the use of the stress method for the extraction of elastic constants to the case of TOECs. Moreover, we show the importance of third-order effects in the strain regimes relevant to a sample InSb/GaSb heterostructure system, and demonstrate for other materials the errors incurred by the use of a linear theory. Finally, our results are compared, where possible, with previous experimental and theoretical results. Overall, we find very good agreement with previously reported experimental and theoretical literature data.

The paper is organized as follows: in Sec. II, we present the finite strain theory in which the TOEC and second-order ISTCs are defined; in Sec. III, we discuss our computational framework, giving the specifics of the DFT implementation and discuss the different nature of convergence of TOECs compared with SOECs, including a comparison of constants extracted from the stress-strain approach with those extracted via the total energy; in Sec. IV, we present the calculated SOECs, TOECs and first- and second-order ISTCs, make comparisons with recent experiment and theory, and apply the extracted TOECs to address the question as to the strain regime in which nonlinear elasticity need be used; finally, in Sec. V, we summarize and conclude.

II. OVERVIEW OF FINITE STRAIN THEORY

In this section, we review the aspects of finite strain theory necessary for the calculation and discussion of TOECs and second-order ISTCs. In Sec. II A, we apply finite strain to the discussion of the macroscopic elasticity of crystals, and in Sec. II B, we outline the theory describing the internal strain resulting from a given applied finite strain.

A. Elasticity

In solid state physics, the description of third-order elasticity is conventionally achieved via the Lagrangian strain formalism [19,28,40,41]. The application of Lagrangian stresses and strains to the theory of elasticity with finite deformations has been developed by Murnaghan [33,34] and applied to cubic crystals by Birch [30].

The deformation gradient tensor F marks the starting point of all strain formalisms. It describes the deformation of a material, including rotations, when the coordinates of that system are transformed. If the position of a point in a material is given by **a**, and after strain is at the position **x**, then the deformation tensor may be defined as [2]

$$F = F_{ij} = \frac{\partial x_i}{\partial a_j}. \tag{1}$$

This relates simply to the linear strain tensor as

$$F_{ij} = \varepsilon_{ij} + \delta_{ij}, \tag{2}$$

where δ_{ij} is the Kronecker delta, and ε is the small, or infinitesimal, strain tensor. While this simple relation between the infinitesimal strain and the deformation is very useful and attractive, the conceptual underpinning of the infinitesimal strain (that it measures the relative changes of lengths in the material) becomes increasingly invalid with increasing strain. Thus, in the regime of larger strains, where third-order elasticity becomes relevant, Lagrangian strains are employed. The Lagrangian strain tensor, η_{ij}, is related to the deformation by [30]

$$\eta_{ij} = \tfrac{1}{2}(F_{ip}F_{jp} - \delta_{ij}), \tag{3}$$

where the Einstein summation notation is used. In cases where the infinitesimal strain tensor is known, the following useful matrix relation may be used to determine the Lagrangian strain tensor [30]:

$$\eta = \varepsilon + \tfrac{1}{2}\varepsilon^2. \tag{4}$$

The TOECs are conventionally defined in terms of the expansion of the free energy density in these Lagrangian strains. For a cubic crystal, this energy density is given by [19,28,30]

$$\begin{aligned}
\rho_0 E &= \tfrac{1}{2}C_{11}\big(\eta_1^2 + \eta_2^2 + \eta_3^2\big) + \tfrac{1}{2}C_{44}\big(\eta_4^2 + \eta_5^2 + \eta_6^2\big) \\
&\quad + C_{12}(\eta_1\eta_2 + \eta_1\eta_3 + \eta_2\eta_3) + \tfrac{1}{6}C_{111}\big(\eta_1^3 + \eta_2^3 + \eta_3^3\big) \\
&\quad + \tfrac{1}{2}C_{112}\big(\eta_2\eta_1^2 + \eta_3\eta_1^2 + \eta_2^2\eta_1 + \eta_3^2\eta_1 + \eta_2\eta_3^2 + \eta_2^2\eta_3\big) \\
&\quad + C_{123}\eta_1\eta_2\eta_3 + \tfrac{1}{2}C_{144}\big(\eta_1\eta_4^2 + \eta_2\eta_5^2 + \eta_3\eta_6^2\big) \\
&\quad + \tfrac{1}{2}C_{155}\big(\eta_2\eta_4^2 + \eta_3\eta_4^2 + \eta_1\eta_5^2 + \eta_3\eta_5^2 + \eta_1\eta_6^2 + \eta_2\eta_6^2\big) \\
&\quad + C_{456}\eta_4\eta_5\eta_6. \tag{5}
\end{aligned}$$

Here, ρ_0 is the mass density of the unstrained material, E is the Helmholtz free energy per unit mass, and the various C_{ij} and C_{ijk} are the second- and third-order isentropic elastic constants, respectively. We have also above employed Voigt [2,45] notation, which, using the symmetry of the strain tensor, makes the convenient contraction of indices: $11 \to 1$, $22 \to 2$, $33 \to 3$, $32 \to 4$, $13 \to 5$, and $12 \to 6$. The derivatives of this energy density, $\rho_0 E$, with respect to the η_i provide equations relating the Lagrangian stresses, t_i, to the Lagrangian strains, η_i, via the elastic constants:

$$t_i = \rho_0 \frac{\partial E}{\partial \eta_i}. \qquad (6)$$

Thus, the general expressions for the Voigt components of the Lagrangian stress in terms of an arbitrary Lagrangian strain on a cubic crystal are

$$
\begin{aligned}
t_1 &= C_{11}\eta_1 + C_{12}(\eta_2 + \eta_3) + \tfrac{1}{2}C_{111}\eta_1^2 + \tfrac{1}{2}C_{112}\big(2\eta_2\eta_1 \\
&\quad + 2\eta_3\eta_1 + \eta_2^2 + \eta_3^2\big) + C_{123}\eta_2\eta_3 + \tfrac{1}{2}C_{144}\eta_4^2 \\
&\quad + \tfrac{1}{2}C_{155}\big(\eta_5^2 + \eta_6^2\big), \\
t_4 &= C_{44}\eta_4 + C_{144}\eta_1\eta_4 + C_{155}(\eta_2\eta_4 + \eta_3\eta_4) + C_{456}\eta_5\eta_6,
\end{aligned}
$$
$$(7)$$

with $t_{2,3}$ and $t_{5,6}$, given by cyclic permutations of the indices of t_1 and t_4, respectively.

However, when the stresses on a strained supercell are calculated via DFT using the Hellmann-Feynman theorem [46] or from an interatomic potential calculation, it is the stresses on the faces of the deformed cell that are obtained; these are the Cauchy stresses, σ. Therefore, in order to use Eq. (7) to extract elastic constants from DFT data, the Lagrangian stress must be related to the Cauchy stress [33]:

$$t = \det(F) F^{-1} \sigma (F^T)^{-1}. \qquad (8)$$

Hence, by either measuring the energy or stress of a cubic crystal as a function of applied Lagrangian strain, Eqs. (5), (7), and (8) may be used to obtain values for the elastic constants. Having established the finite strain formalism required for the discussion of TOECs, in the next section we describe the application of this formalism to the description of nonlinear inner elasticity in cubic crystals.

B. Internal strain

Nonlinear internal strain involves a second, rather than first-order description of the internal strain in terms of the Lagrangian strain. To achieve this description of sublattice displacement to second order in the regime of large strains for ZB semiconductors, we will use the formalism introduced by Cousins [10,27].

Taking the ZB primitive cell, and letting the atom at the origin remain fixed, the position of the second atom, after strain, is given by

$$\mathbf{r} = F\mathbf{r}_0 + \mathbf{u}, \qquad (9)$$

where $\mathbf{r}_0$ is its equilibrium position and $\mathbf{u}$ represents the internal strain vector. Although this transformation completely specifies the deformed positions geometrically, the $\mathbf{u}$ are not suitable parameters in which to expand the scalar energy.

This is because they lack rotational invariance. Given that the internal strain represents the atomic configuration which minimises the energy of the ZB crystal under shear strain, a rotationally invariant description of the internal strain is needed. This is obtained through use of what Cousins [10] calls the *inner displacement*. This is given by

$$\boldsymbol{\xi} = F^T \mathbf{u}. \qquad (10)$$

Because this inner displacement occurs in response to internal forces arising from the application of finite strain, each inner displacement can be expressed as a Taylor series in the components of the strain:

$$\xi_i = A_{iJ}\eta_J + \tfrac{1}{2}A_{iJK}\eta_J\eta_K. \qquad (11)$$

Here, Voigt notation has been employed for the elements of the finite strain tensor, and the Einstein summation convention is again utilised. The subscripts relating to the strain are denoted by capitals, whilst those relating to the Cartesian coordinate of the inner displacement are denoted by the lower case i. The A_{iJ} and A_{iJK} are the first- and second-order *internal strain tensors*, respectively. Cousins [27,47] gives the form of these tensors for a ZB crystal. The first-order internal strain tensor may be expressed conveniently in matrix notation:

$$A_{iJ} = \begin{pmatrix} 0 & 0 & 0 & A_{14} & 0 & 0 \\ 0 & 0 & 0 & 0 & A_{14} & 0 \\ 0 & 0 & 0 & 0 & 0 & A_{14} \end{pmatrix}. \qquad (12)$$

We note that for small strains, $F \approx I$, the identity matrix, and $\boldsymbol{\xi} \approx \mathbf{u}$, where $u_i = -\frac{a_0}{2}\zeta\varepsilon_{jk}$ ($u_1 = -\frac{a_0}{2}\zeta\varepsilon_{23}$, $u_2 = -\frac{a_0}{2}\zeta\varepsilon_{13}$, $u_3 = -\frac{a_0}{2}\zeta\varepsilon_{12}$), and thus $A_{14} = -\frac{a_0}{4}\zeta$, where ζ is the well known Kleinman parameter [9].

A matrix representation is not possible for A_{iJK}, but there are only three independent nonzero components, which are [47]

$$A_{114} = A_{225} = A_{336}, \qquad (13)$$

$$A_{156} = A_{246} = A_{345}, \qquad (14)$$

$$A_{124} = A_{235} = A_{316} = A_{134} = A_{215} = A_{326}. \qquad (15)$$

Substituting Eqs. (12)–(15) into Eq. (11) yields an expression for the value of $\boldsymbol{\xi}$, which minimises the strain energy of a ZB crystal for a given applied finite strain:

$$
\boldsymbol{\xi} = A_{14}\begin{pmatrix} \eta_4 \\ \eta_5 \\ \eta_6 \end{pmatrix} + \frac{A_{114}}{2}\begin{pmatrix} \eta_1\eta_4 \\ \eta_2\eta_5 \\ \eta_3\eta_6 \end{pmatrix} \\
+ \frac{A_{124}}{2}\begin{pmatrix} \eta_4(\eta_2 + \eta_3) \\ \eta_5(\eta_3 + \eta_1) \\ \eta_6(\eta_1 + \eta_2) \end{pmatrix} + \frac{A_{156}}{2}\begin{pmatrix} \eta_5\eta_6 \\ \eta_4\eta_6 \\ \eta_4\eta_5 \end{pmatrix}. \qquad (16)
$$

If, for a given primitive ZB unit cell, the atomic positions corresponding to the energetic minimum for a particular Lagrangian strain branch are known, Eq. (16) can be used in fitting procedures to obtain the first- and second-order ISTCs.

In the next section, the manner in which the presented finite strain theory is applied to deformed unit cells is described. In addition, the details of the DFT caculations performed to

obtain the stresses on, and energies of, these deformed unit cells are presented, along with a discussion of the different calculational criteria needed for the accurate calculation of elastic constants and internal strain tensor components.

III. COMPUTATIONAL METHOD

In this section, we discuss the computational method used to calculate the SOECs, TOECs, and first- and second-order ISTCs.

First, in Sec. III A, the deformations applied to each ZB unit cell are presented. This is accompanied by a description of the strains and stresses associated with these deformations via the finite strain theory introduced in the previous section. In Sec. III B, the details of the DFT calculations are given. This is followed in Sec. III C by an analysis of the convergence of the calculations with respect to k-point grid density, plane-wave cutoff energy, lattice constant, and applied strain range. In particular, it is demonstrated and explained that a higher resolution of calculation in terms of k-point grid density, cutoff energy, and lattice constant, is needed to achieve convergence of TOECs when compared with that needed for the calculation of SOECs. Whether to calculate the elastic constants via the calculated stresses or energies is discussed. Our results show that, using the energy method, the convergence of TOECs is much slower with respect to cutoff energy, k points, and applied strain range when compared to that exhibited by the stress strain method. Consequently, the energy method is significantly more computationally expensive. A similar behavior has been reported in the literature for SOECs [48], where it was identified that the slower convergence of the energy method occurs due to changes in the k-point basis set used, as the cutoff energy is kept fixed in the calculations, while the unit cell size/shape is being varied. By contrast, the stresses, when calculated according to the Hellmann-Feynmann theorem, are computed implicitly for a fixed basis set (since they are computed at fixed lattice vectors). We then find, given the already high computational demands, that the effect of the changing basis set in the energy calculations is strongly enhanced when calculating TOECs, as further discussed in Sec. III C 1.

A. Applied deformations

For the extraction of all SOECs, TOECs, and first- and second-order ISTCs, data from the following applied strain branches [24] were used:

$$\boldsymbol{\epsilon}^{(1)} \equiv (0, 0, 0, \beta, \beta, \beta),$$
$$\boldsymbol{\epsilon}^{(2)} \equiv (\alpha, 0, 0, \beta, 0, 0),$$
$$\boldsymbol{\epsilon}^{(3)} \equiv (0, \alpha, 0, \beta, 0, 0), \qquad (17)$$
$$\boldsymbol{\epsilon}^{(4)} \equiv (0, \alpha, \alpha, \beta, 0, 0),$$
$$\boldsymbol{\epsilon}^{(5)} \equiv (\alpha, \alpha, \alpha, \beta, \beta, \beta).$$

The corresponding deformations of the unit cell were chosen such that, according to the symmetries of Eqs. (12)–(16), at least one independent determination of each of the second-order ISTCs would be obtained from the resultant inner displacements. Deformations chosen in this way also enabled

several pathways to the determination of each of the SOECs and TOECs from the stresses on the unit cells.

For the calculation of all elastic constants and ISTCs, α and β are varied in the following manner: In the strain branch $\boldsymbol{\epsilon}^{(1)}$, β is varied in steps of 0.01 from -0.04 to 0.04, resulting in a total of 9 strain points. For each of the remaining branches, α (β) is varied from -0.02 (-0.04) to 0.02 (0.04) in steps of 0.01 (0.02), comprising a total of 25 points. Each value of α and β is associated with six stress components, a total energy value, and the position vectors of the atoms in the ZB primitive cell. To ascertain the form of the relation between the deformation parameters α and β, and the stress, energy, and relaxed atomic positions, the Lagrangian strains corresponding to each deformation branch must be determined. Using the tensor relation, Eq. (4), the Lagrangian strains, $\boldsymbol{\eta}^{(i)}$, obtained from the strain branches, $\boldsymbol{\epsilon}^{(i)}$, are given by

$$\boldsymbol{\eta}^{(1)} \equiv \left(\frac{\beta^2}{4}, \frac{\beta^2}{4}, \frac{\beta^2}{4}, \beta + \frac{\beta^2}{4}, \beta + \frac{\beta^2}{4}, \beta + \frac{\beta^2}{4} \right),$$

$$\boldsymbol{\eta}^{(2)} \equiv \left(\alpha + \frac{\alpha^2}{2}, \frac{\beta^2}{8}, \frac{\beta^2}{8}, \beta, 0, 0 \right),$$

$$\boldsymbol{\eta}^{(3)} \equiv \left(0, \alpha', \frac{\beta^2}{8}, \beta + \frac{\alpha\beta}{2}, 0, 0 \right), \qquad (18)$$

$$\boldsymbol{\eta}^{(4)} \equiv (0, \alpha', \alpha', \beta + \alpha\beta, 0, 0),$$

$$\boldsymbol{\eta}^{(5)} \equiv \left(\alpha' + \frac{\beta^2}{8}, \alpha' + \frac{\beta^2}{8}, \alpha' + \frac{\beta^2}{8}, \beta', \beta', \beta' \right),$$

where the notation $\alpha' = \alpha + \frac{\alpha^2}{2} + \frac{\beta^2}{8}$ and $\beta' = \beta + \frac{\beta^2}{4} + \alpha\beta$, has been used for compactness.

With these five strain branches there are five energy equations from Eq. (5), from which all SOEC and TOECs may be obtained, fourteen unique stress component equations, from which all SOEC and TOEC may be obtained in multiple ways using Eqs. (7), and five equations for inner displacements, from Eq. (16). We do not present these twenty four long equations here in the interest of brevity. However, to illustrate the methodology, we will present in the Results section a sample subset of these equations, truncated to second order in the deformation parameters. A more detailed description of the full set of stress and inner displacement fitting equations is given in Ref. [49].

The first three of the Lagrangian strain branches of Eq. (18) allow, via the relaxed atomic positions, determination of A_{14} (the Kleinman parameter within the finite strain formalism, $\approx -\frac{\zeta a_0}{4}$), and all three of the second-order ISTCs. Furthermore, because α and β are varied independently, these first three branches also furnish, via the different components of the stress tensor, multiple independent determinations of each of the SOECs, and all but one of the TOECs. The remaining TOEC, C_{123}, can then be determined from the stress in the x direction associated with $\boldsymbol{\eta}^{(4)}$. The stresses and relaxed atomic positions of the more complicated strain branch, $\boldsymbol{\eta}^{(5)}$, are not used to obtain any new values for the elastic constants, but to check the overall accuracy and consistency of the full set of elastic constants or ISTCs by substituting in particular values derived from the other branches, and performing fits for the remaining constants. Since the fitting will be dependent on the accuracy of the substituted constants, the agreement of the

result with previous fittings indicates accurate determination of all those substituted constants, as well as those newly obtained.

B. DFT framework for the calculation of energy, stress, and relaxed atomic positions

To obtain the energies, stresses, and relaxed atomic positions associated with each of the above strain branches, DFT calculations were performed on the (deformed) ZB unit cells using the Heyd-Scuseria-Ernzerhof (HSE) hybrid-functional approach [44]. The calculations were carried out using the software package VASP [50]. A screening parameter, μ, of $0.2\,\text{Å}^{-1}$, and an exact exchange mixing parameter, α, of 0.25, were utilized; these correspond to VASP's HSE06 version of the HSE functional. More details are given in Ref. [24].

For the calculation of material parameters, DFT within the HSE scheme offers improved accuracy over standard Kohn-Sham approaches to the exchange energy [51]. For instance, it circumvents the well known band gap problem of LDA and generalised gradient approximation (GGA) implementations. Moreover, HSE-DFT has been shown to give improved predictions of elastic and lattice properties of solids over LDA and GGA implementations [52,53]. Fitting to the DFT data using Eqs. (5), (7), and (16), yields values for the SOECs and TOECs as well as first and second-order ISTCs as described above.

For the determination of elastic constants, we choose to fit to the stress-strain equations [Eq. (7)] rather than the energy-strain equations [Eq. (5)] for reasons of greater accuracy and efficiency [40,41,46,48], which we will demonstrate below. In general, the stress method is suited to efficient calculation of the elastic constant tensor because a single DFT calculation yields the full stress tensor, with its six unique components, and six equations to fit to. However, a single DFT calculation produces only one scalar energy, with one equation available to fit to. Thus the elastic constants can be obtained via the stress method efficiently from one calculation, whereas from the energy method, several separate calculations are needed for the same number of constants. Furthermore, in terms of accuracy, the equations relating these elastic constants to the strains will be a lower-order polynomial in the strain, and therefore easier to fit when dealing with very small strains. Finally, as will be corroborated in the next section: in a plane wave-based DFT implementation using a fixed cutoff energy in its plane-wave expansion at different k-points and different lattice vectors, the number of k points and cutoff energy needed in a given calculation to obtain converged values of the elastic constants is lower for those calculated via the stress method than for those calculated via the total energy method [48]. Consequently, elastic constants can be determined to a desired accuracy at less computational expense using the stress method. Moreover, these issues of convergence are even more pronounced for TOECs and second-order ISTCs than SOECs and first-order ISTCs, as will be demonstrated below.

C. Convergence of results

In this section, we analyze the convergence of our results, and show that the aforementioned advantages in convergence

which the stress method exhibits over the energy method, demonstrated in the literature in the context of SOECs [40,46,48] are even more dramatic for the TOECs. First, in Sec III C 1, we show that TOECs require a higher resolution of calculation than SOECs: that elastic constants extracted via the stress method converge faster with respect to k-point mesh density and cutoff energy than those extracted via the energy method; and that the elastic constants presented here, calculated using the stress method, are converged (where those extracted via the energy method, from the same calculation, may not be). These convergence tests are shown using InSb as a model system, which of the studied materials is the slowest to converge with k-point density and cutoff energy. Thus, the presented results for InSb validate also the convergence of the other III-V materials studied here. Second, in Sec. III C 2, the dependence of the extracted elastic constants on the equilibrium pressures and applied strain ranges is investigated. The increased sensitivity of TOECs to these calculation parameters when compared with SOECs is highlighted, and this increased sensitivity is shown to be worsened when elastic constants are extracted through use of the energy method. Finally, the suitability of our choice of applied strain range and allowed equilibrium pressure are confirmed.

1. Convergence with k points and cutoff energy

Compared to the effects of linear elasticity, third-order elasticity gives rise to smaller changes in stress, energy, and atomic positions. Therefore it can be expected that convergence of TOECs will require denser k-point grids and higher cutoff energies than is the case for SOECs. We find that this is, indeed, the case, as illustrated in Fig. 1, where, for InSb, the slower convergence of the stress-extracted TOECs with respect to k-point density may be immediately inferred from the different scales. Here, the cutoff energy is fixed at 600 eV. On closer inspection of Fig. 1, one finds that the percentage changes in C_{11} and C_{12} on going from a $6 \times 6 \times 6$ to an $8 \times 8 \times 8$ k-point grid are both 1%, whilst for C_{111} and C_{112} the values change by 10% and 17%, respectively. Therefore, while an $8 \times 8 \times 8$ k-point grid may be sufficient to obtain converged SOECs, the calculation of TOECs requires a higher k-point density. Examining the percentage change in the calculated constants when going from an $8 \times 8 \times 8$ to a $10 \times 10 \times 10$ k-point mesh, convergence of both SOECs and TOECs is apparent. For the SOECs, a negligible difference of 0.5% exists, whilst for the TOECs, C_{111} and C_{112}, the values differ by only 4% and 5%, respectively. To further corroborate convergence of the TOECs, we note the negligible change on increasing the k-point density from $10 \times 10 \times 10$ to $12 \times 12 \times 12$; the differences being <1% for both TOECs. With these small changes between subsequent grid sizes, we conclude that a grid of $10 \times 10 \times 10$ is sufficient to converge the stress extracted elastic constants, at a cutoff energy of 600 eV.

While Fig. 1 establishes convergence of the elastic constants extracted through the stress method, Fig. 2 justifies the choice of extracting the elastic constants using the stress rather than energy by showing the poorer convergence of the energy method. Figure 2 shows that, using the energy method, the TOECs also converge much slower when
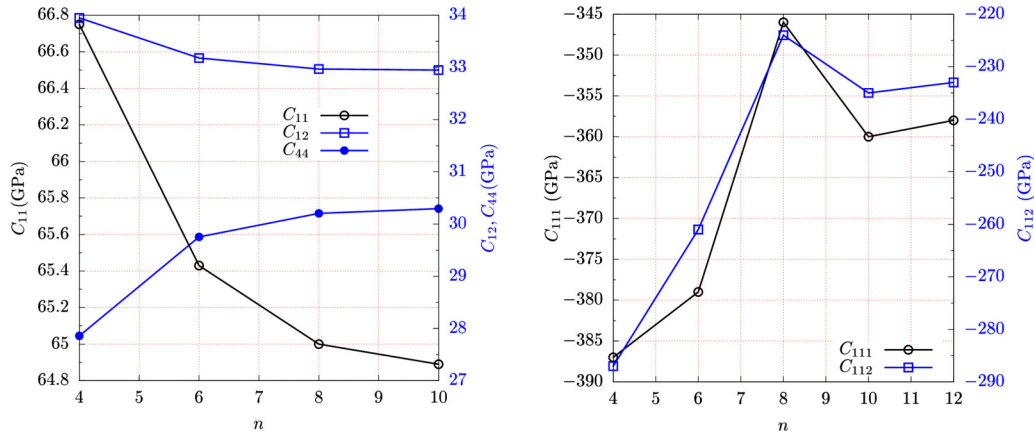
FIG. 1. Comparison of convergence with k-point density of *stress-extracted* InSb SOECs (left) and TOECs (right). The calculations were performed at a cutoff energy of 600 eV, on a k-point grid of $n \times n \times n$, with C_{11}, C_{12}, C_{111}, and C_{112} all determined from an applied strain of $\epsilon = (\alpha, 0, 0, 0, 0, 0)$, with α varied between $\pm 2\%$ in steps of 1% and C_{44} is determined via a shear strain $\epsilon = (0, 0, 0, \beta, \beta, \beta)$, with β varied between $\pm 4\%$ in steps of 2%.

compared with the SOECs. Also similarly to the convergence of the stress-extracted constants, the energy-extracted TOECs are also clearly converged with respect to k-point density by a $10 \times 10 \times 10$ k-point grid density. However, in this case, the TOECs exhibit much larger fluctuations at lower grid densities. For example, at a grid of $4 \times 4 \times 4$, the energy extracted C_{111} is 28% lower than the converged value, whilst the stress-extracted $4 \times 4 \times 4$ C_{111} is only 8% lower than its converged value. In addition to the fact that the energy values are converging slowly, we note, more importantly, that they are also unconverged at this cutoff energy, with final C_{111} and C_{112} values of -504 and -242 GPa, respectively, compared to the converged stress-extracted values of -360 and -235 GPa.

Therefore, in a second step, we analyze the impact of the cutoff energy on the elastic constants. Table I shows the effect of increasing the cutoff energy, with a fixed k-point grid of $10 \times 10 \times 10$, on the calculated C_{11} and C_{111} values. The superscripts t and E refer to constants extracted via the stress and energy methods, respectively. The numbers following

the "$\pm$" are the fitting errors. The table shows that for both the energy and stress method, a cutoff of 400 eV is more than sufficient to obtain converged SOECs. However, for the TOEC C_{111}, only the stress extracted C_{111} is converged. As with Figs. 1 and 2, the table shows that TOECs generally require higher cutoff energies than SOECs; energy extracted TOECs require higher cutoff energies for a given accuracy than stress extracted TOECs; that a cutoff energy of 600 eV is sufficient to obtain converged TOECs (for InSb) using the stress method; and that even for a cutoff energy of 1000 eV, the energy method still does not yield a converged value for C_{111}^E, as can be seen by comparison with C_{111}^t.

The slower convergence of the energy extracted parameters with respect to those extracted via the stresses is due to the larger impact of the changing plane-wave basis set on the strain energy than on the stress [48]. The total energy results can in principle be corrected by using a (in general anisotropic) strain-dependent cutoff energy. For small strains, $\pm 1\%$ change in lattice vectors corresponds to $\sim \mp 2\%$ change in cutoff energy. This is because, for a cutoff energy E_{cut}, only
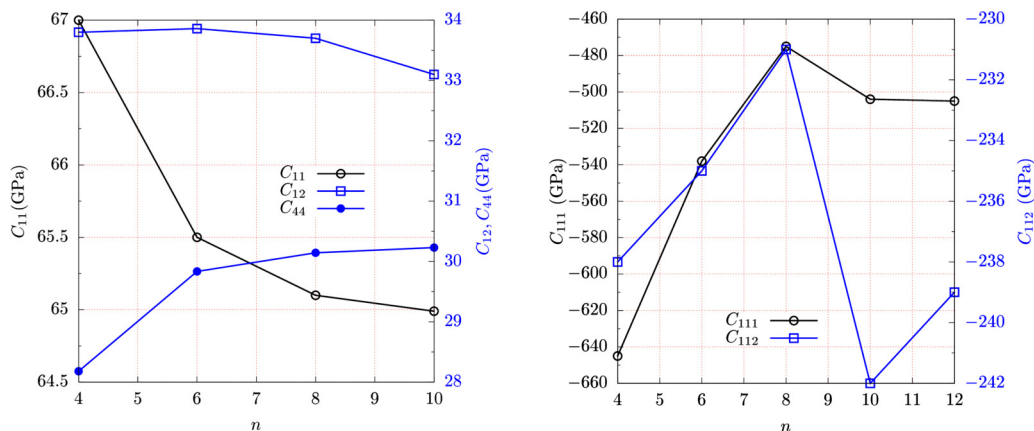
FIG. 2. Convergence with k-point density of InSb (left) SOECs and (right) TOECs *extracted using the energy method*. The calculations were performed at a cutoff energy of 600 eV, on an $n \times n \times n$ k-point grid. C_{11}, C_{12}, C_{111}, and C_{112} are all determined from an applied strain of $\epsilon = (\alpha, 0, 0, 0, 0, 0)$, with α varied between $\pm 2\%$ in steps of 1% and C_{44} is determined via a shear strain $\epsilon = (0, 0, 0, \beta, \beta, \beta)$, with β varied between $\pm 4\%$ in steps of 2%.

TABLE I. Effect of cutoff energy on elastic constants, C_{11} and C_{111}, of InSb calculated using the stress and energy method. A superscript of t denotes the stress method, and E denotes the energy method. Calculations all performed with a k-point grid of $10 \times 10 \times 10$.

E_{cut} (eV)	C_{11}^t (GPa)	C_{11}^E (GPa)	C_{111}^t (GPa)	C_{111}^E (GPa)
400	65.2 ± 0.1	65 ± 1	-379 ± 11	-1108 ± 15
600	64.89 ± 0.03	65.0 ± 0.2	-360 ± 4	-504 ± 34
1000	64.8 ± 0.1	64.9 ± 0.1	-359 ± 6	-445 ± 21

those plane waves that obey the condition $|\mathbf{G} + \mathbf{k}| < G_{\text{cut}}$, where $\mathbf{G}$ is a reciprocal lattice translation, are included in the basis, with

$$E_{\text{cut}} = \frac{\hbar^2}{2m} G_{\text{cut}}^2. \tag{19}$$

Modifying the cut-off energy to maintain a fixed basis set leads to a remarkably improved agreement between total energy and stress methods, as shown in Fig. 3, where to illustrate this point, we have performed LDA calculations of the bulk modulus of AlN using energy and stress, with and without the cutoff energy correction.

Unfortunately, this cut-off energy correction can only be easily implemented for hydrostatic strain (i.e., only allows to calculate bulk modulus) because this is the only case where the basis set changes isotropically, consistent with Fig. 3. Because it avoids these issues, the stress method should therefore be used for reliable, consistent, and computationally inexpensive calculation of elastic constants.

Finally, we note that InSb, being the heaviest and softest material, will require the highest resolution of calculation in terms of cutoff energy and k-point mesh. Thus the convergence indicated in Fig. 1 and Table I also serves to confirm that the chosen cutoff energy and k-point density are appropriate for the other materials.

2. Convergence with applied strain range and equilibrium pressure

In addition to their sensitivity to k-point grid density and cutoff energy, TOECs also exhibit a more pronounced dependence on the residual pressure at the assumed equilibrium lattice constant, and the range of strain applied to the system

TABLE II. Effect of residual pressure due to insufficient lattice relaxation on C_{111} and C_{11} of AlN. The accompanying errors are the least squares fitting errors. C_{111}' is the value for C_{111} extracted using a fitting, which accounts for the equilibrium pressure. The calculations were performed with a cutoff energy of 600 eV and a k-point grid density of $10 \times 10 \times 10$.

a_0 (Å)	P_0 (kB)	C_{11} (GPa)	C_{111} (GPa)	C_{111}' (GPa)
4.3643	0.5927	310 ± 3	-1471 ± 169	-1122 ± 3
4.3646	0.1521	309.56 ± 0.40	-1212 ± 43	-1123 ± 3
4.3647	0.0051	309.49 ± 0.03	-1125 ± 3	-1122 ± 3
4.3648	-0.1369	309.41 ± 0.37	-1037 ± 40	-1118 ± 3
4.3651	-0.5752	309 ± 2	-778 ± 164	-1117 ± 4

in order to calculate them. Because the demonstration of this point requires a large number of calculations, in this section we analyze the TOECs and SOECs of AlN. For this compound of lighter atoms, the stress and total energy calculations are computationally less expensive than for InSb. Unless stated otherwise, all convergence tests are performed at a cutoff energy of 600 eV and on a $10 \times 10 \times 10$ k-point mesh.

The issue of lattice constant relaxation is examined in Table II, where the elastic constants C_{11} and C_{111}, extracted using the stress method, are shown for different equilibrium lattice constants and pressures. The C_{111} and C_{11} values displayed are the result of applying the strain branch $\boldsymbol{\varepsilon} = (\alpha, 0, 0, 0, 0, 0)$ with α varied from -0.02 to 0.02 in steps of 0.01. The pressure denoted by P_0 in the table is the calculated residual pressure on the ZB primitive cell with the lattice constant given in the first column. The values preceded by the "$\pm$" are least squares fitting errors.

Table II shows that, when optimizing the lattice constant by minimizing the absolute value of the pressure on the unit cell, the magnitude of the pressure below which we may accurately extract elastic constants from the stress, using standard fitting methods, is lower for TOECs than for SOECs. In columns three and four of Table II are presented the results of fitting the equation $t_1 = (\frac{C_{111}}{2} + \frac{C_{11}}{2})\alpha^2 + C_{11}\alpha$ directly to the DFT data, which include this 'equilibrium' pressure, P_0, as the pressure corresponding to a strain of 0%. Here the variation of AlN's C_{111} value with residual "equilibrium" pressure may be contrasted with the constancy of the corresponding C_{11} value. As the residual pressure increases, so does the value of
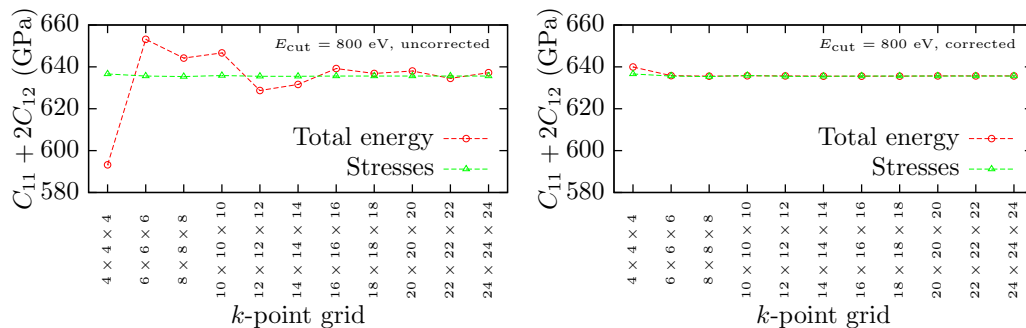

FIG. 3. LDA calculation of the bulk modulus ($C_{11} + 2C_{12}$) of AlN, using both the stress and energy method. (left) Results for a fixed cutoff energy of 800 eV, and (right) with a strain-corrected cutoff around 800 eV, for the same system (hydrostatically strained ZB AlN).

TABLE III. Impact of range of applied strain in fitting data for AlN on SOEC C_{11}^t extracted from the stresses, and TOECs C_{111}^t and C_{111}^E extracted from the stresses and energy, respectively. All elastic constants are in units of GPa. C_{11}^t, C_{111}^t, and C_{111}^E are calculated on a k-point grid of density $10 \times 10 \times 10$, and with a cutoff energy of 600 eV. C_{111}^E (1000 eV) has the same settings but with the cutoff energy increased to 1000 eV.

$\alpha_{\max}$	C_{11}^t	C_{111}^t	C_{111}^E	C_{111}^E (1000 eV)
$\pm 2\%$	309.49 ± 0.03	-1125 ± 3	-2959 ± 381	-1223 ± 22
$\pm 4\%$	310.0 ± 0.1	-1125 ± 6	-1627 ± 80	-1153 ± 6
$\pm 6\%$	310.8 ± 0.2	-1126 ± 8	-1359 ± 31	-1137 ± 5
$\pm 8\%$	311.9 ± 0.3	-1128 ± 9	-1261 ± 17	-1132 ± 5

C_{111} deviate from the value obtained at lowest pressure, along with increasing fitting errors. For a lattice constant change of -0.0004 Å from the lowest pressure lattice constant, a 30% error is incurred in C_{111}. This may be attributed to related factors such as: the small magnitudes of the contribution of the TOEC to the total stress (at $\alpha = 0.02$, $\frac{C_{111}}{2}\alpha^2 = 2.25$ kB), of which the initial pressure is a significant fraction; and the tendency of higher-order polynomials to be more sensitive to noise in fitting.

The errors so-incurred can be reduced by two means. The first is to modify the fitting equation to account for the equilibrium pressure; i.e., by fitting using the equation: $t_1 = (\frac{C'_{111}}{2} + \frac{C_{11}}{2})\alpha^2 + C_{11}\alpha + P_0$. The improvements induced by this adjustment are evident in the stability with intial pressure of C'_{111} in column five of Table II. The second way to reduce these errors is to ensure the lattice has been relaxed to a sufficiently low pressure. While the origin adjustment shown before more than solves the problem for AlN over the given pressure range, for softer materials, this sensitivity to initial pressure will be even more pronounced, with a given pressure corresponding to a higher strain, and this adjustement is less effective. We thus impose more stringent criteria on the maximum pressures below which we consider a crystal to be relaxed, aiming for pressures below 0.1 kB, a fifth of the cutoff value of $\sim$0.5 kB typically used for SOECs [54].

Another important calculation parameter to which the TOECs are sensitive is the range of strain applied to the unit cell [41,54]. Applying strains over a larger range will produce larger changes in stress and energy from which the contribution of the third-order terms will be more easily discerned; however, as the strain range is increased, even higher-order terms may begin to have an effect. Furthermore, having a large strain range with a constant strain point density will require a larger number of calculations. Thus, the strain range applied will need to be large enough that the effect of the TOECs can be observed, but not so large that further higher-order terms come into play, or the calculation is prohibitively expensive; i.e., the optimal strain range is the minimum strain range at which the effects of TOECs are appreciable.

Table III shows the influence of the range of applied strain on the calculated elastic constants of AlN. The superscript t in this table refers to a stress extracted constant, and E denotes an energy extracted constant. $\alpha_{\max}$ denotes the maximum value of α in the applied strain of $\boldsymbol{\varepsilon} = (\alpha, 0, 0, 0, 0, 0)$, with

the data set comprising strains in increments of 1% between $\pm\alpha_{\max}$. The stability of the stress extracted C_{11}^t and C_{111}^t in Table III reveals that the range of $\pm 2\%$ is large enough to yield measurable nonlinearities in the stress, but not so large that higher-order terms interfere with the fitting. The increasing influence of these unwanted higher-order terms can be observed in the increasing errors of C_{111}^t. The rightmost two columns of the table show again the shortcomings of the energy method when compared with the stress method for the extraction of TOECs; the energy extracted constants requiring larger strain ranges to lower the fitting error. The rightmost column shows the interrelation between the cutoff energy and the strain range. Small errors in the calculated free energy can have significant impact on the determined TOECs at small strain; increasing the cutoff energy reduces the scale of these errors, while increasing the strain range reduces their relative input in the total calculated change in energy. Overall, we see that the convergence of the TOEC values is clearly slower using the energy method.

Having justified our choice of the stress method over the energy method for the extraction of SOECs and TOECs, and shown that our stress extracted constants are indeed converged, we present in the next section the full set of SOECs and TOECs for all considered materials, and discuss the results.

IV. RESULTS

In this section, the calculated SOECs, TOECs, and first and second-order ISTCs are presented and discussed. First, in Sec. IV A, the calculated elastic constants are presented, along with plots validating the fittings used to obtain them. The extracted values are compared with previous experimental and theoretical literature results, and an analysis of the strains at which third-order effects become important is made. In Sec. IV B, the calculated first and second ISTCs are reported.

A. Elastic constants

Given below in Eqs. (20) and (21), are six sample stress fitting equations, truncated to second-order in the strain, each furnishing an independent determination of a subset of the nine independent elastic constants of a ZB crystal. Equations (20) show three axial stress equations which may be used to determine simultaneously the SOECs, C_{11} and C_{12}, and the TOECs, C_{111}, C_{112}, and C_{123},

$$t_1^{(2)}(\alpha, 0) = \tfrac{1}{2}(C_{11} + C_{111})\alpha^2 + C_{11}\alpha,$$
$$t_2^{(2)}(\alpha, 0) = \tfrac{1}{2}(C_{12} + C_{112})\alpha^2 + C_{12}\alpha, \qquad (20)$$
$$t_1^{(4)}(\alpha, 0) = (C_{12} + C_{112} + C_{123})\alpha^2 + 2C_{12}\alpha,$$

and Eq. (21) shows three shear stresses that yield simultaneously values of the SOEC C_{44}, and TOECs C_{144}, C_{155}, and C_{456}:

$$t_4^{(2)}(\alpha, \beta) = C_{144}\alpha\beta + C_{44}\beta,$$
$$t_4^{(3)}(\alpha, \beta) = \left(\tfrac{1}{2}C_{44} + C_{155}\right)\alpha\beta + C_{44}\beta,$$
$$t_4^{(1)}(\beta) = \left(\tfrac{1}{4}C_{44} + C_{456}\right)\beta^2 + C_{44}\beta. \qquad (21)$$
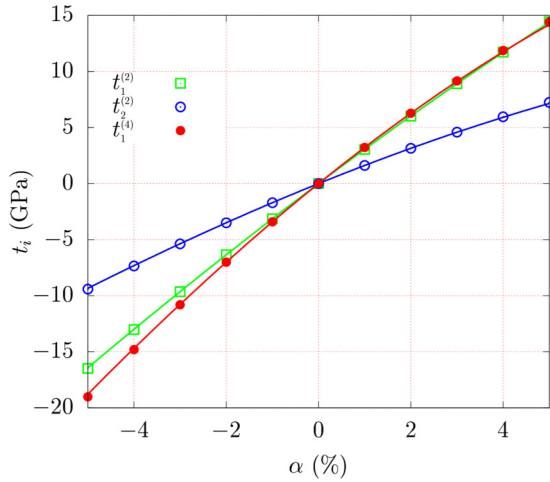
FIG. 4. Fitting Lagrangian stresses of Eq. (20) to AlN HSE-DFT data. The points represent calculated DFT data, and the lines depict stresses determined from Eqs. (20). The used elastic constants defining the functions in Eq. (20) are obtained by fitting to the data out to $\pm 2\%$, and are presented in Table V.

Here, the subscripts on the $t_i^{(n)}$ refer to the stress tensor component in Voigt notation, and the superscripts, n, refer back to the strain branches, $\boldsymbol{\eta}^{(n)}$, in Eq. (18). The zeros in brackets in Eq. (21) indicate that β is set to 0, and only α is varied.

The solid lines in Figs. 4 and 5 show the stresses on AlN unit cells as a function of strain, calculated using the expressions in Eqs. (20) and (21). The figures also display the stresses calculated by DFT for each strain (symbols). Note that the fitting of the coefficients in Eqs. (20) and (21) is not done on the data sets shown in the figure. These coefficients were obtained by two-dimensional fittings to unsimplified un-
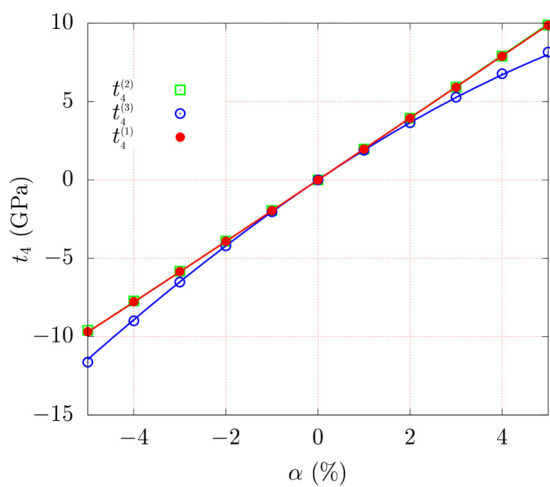

FIG. 5. Fitting shear stresses of Eqs. (21) to one dimensional line scans of AlN HSE-DFT data. Here the data plotted are on the line $\alpha = \beta$. The points represent calculated DFT data points, and the lines represent stresses calculated via Eq. (21), with coefficients fitted from data sets with $-2\% < \alpha < 2\%$ and $-4\% < \beta < 4\%$, using elastic constants presented in Table V.

truncated stress equations using only data points in the range $-2\% \leqslant \alpha \leqslant 2\%$ and $-4\% \leqslant \beta \leqslant 4\%$. The lines shown in the figure show then predictions for higher strain values. As the figures confirm, not only is the fit very good at $\pm 2\%$, but the line also matches the DFT data points very well at higher strains. The influence of nonlinear effects may be inferred from the slight curvature and asymmetry of the lines.

By performing fittings to several stress relations, the full set of SOECs and TOECs for all considered materials were obtained. For C_{11} and C_{111}, there are two independent determinations, from $t_1^{(2)}$ and $t_2^{(3)}$, and the values given in Tables IV and V are the averages of these two. The constants C_{12} and C_{112} have three independent determinations, $t_{2,3}^{(2)}$, $t_1^{(3)}$ and the values given in the table are the averages of these. C_{123} is obtained from the single fitting to $t_1^{(4)}$. For C_{155}, we extracted six separate values from the different stresses on the unit cells; the value given is the average of all these very closely agreeing values. C_{144} is given as an average over the values obtained from the three stresses $t_1^{(2)}$, $t_4^{(2)}$, and $t_1^{(3)}$. Finally, for all materials, C_{44} and C_{456} were obtained from $t_4^{(1)}$.

Table IV presents a comprehensive comparison with experiment and previous theory of lattice constants, SOECs, and Kleinman parameters for all considered materials. The table reveals an abundance of both experimental and theoretical values of lattice and elastic constants for all materials except for the metastable III-N compounds and highly toxic AlP, for which experimental elastic constants are not available. For the Kleinman parameter, experimental values are rare, with measurements made only on GaAs [69] and InSb [36]. The theoretical values presented are from DFT studies utilising different approximations to the exchange correlation energy functional. References [43,55,56,59,61,64] use the local density approximation (LDA) to the exchange correlation functional. As is evident from the table, in most cases, LDA DFT accounts well for the elastic properties of solids; however, LDA is known to often overestimate the binding in solids [53], resulting in smaller lattice and larger elastic constants. Indeed, we see from Table IV that whenever there is a significant disagreement between LDA elastic or lattice constants and those experimentally measured or here calculated, the LDA elastic constants tend to be larger. For the Al containing compounds considered here, this trend seems not to hold, with the elastic constants being often smaller than experiment, but nevertheless agreeing very closely. References [18,19] use the generalised gradient approximation (GGA) of Purdew, Burke, and Ernzerhof (PBE) [72]. This functional tends to underestimate binding energies [19,53], and examining in particular InAs and GaAs, we see this trend borne out. From Ref. [53], we take those structural and elastic properties calculated using HSE; these show good agreement with the HSE-DFT values of the present study, as well as with experimental values. This good agreement with experiment demonstrates both the validity of the particular HSE-DFT determined elastic constants presented here, and of the use of this method for the calculation of structural and elastic properties in general.

The TOECs, averaged over the independent determinations given in Eqs. (7) and (18), are gathered in Table V. The errors following the constants are the fitting errors.

TABLE IV. Elastic and structural properties of III-V compounds, where C_{ij} are the second-order elastic constants, a_0 is the equilibrium lattice constant, and ζ is Kleinman's internal strain parameter. All calculations have been performed with a cutoff energy of 600 eV, on a k-point grid density of $10 \times 10 \times 10$, and the stress method is used to obtain the elastic constants.

		a_0 (Å)	C_{11} (GPa)	C_{12} (GPa)	C_{44} (GPa)	ζ
	Prev. theory	4.342 [55]	304 [56], 282 [19]	160 [56], 149 [19]	193 [56], 179 [19]	0.55 [56]
AlN	Experimental	4.373 [57], 4.38 [58]	–	–	–	–
	Present	4.3647	309.47	166.06	196.90	0.5385
	Prev. theory	5.417 [59], 5.4735 [60]	132.5 [61]	66.7 [61]	62.7 [61]	0.604 [61]
AlP	Experimental	5.46 [62], 5.4635 [63]	–	–	–	–
	Present	5.4713	138.25	67.73	66.52	0.5759
	Prev. theory	5.614 [59]	113.1 [61]	55.5 [61]	54.7 [61]	0.592 [61]
AlAs	Experimental	5.66139 [63]	119.9 [63]	57.5 [63]	56.6 [63]	–
	Present	5.6865	116.64	55.62	56.96	0.5746
	Prev. theory	6.090 [59]	85.5 [61]	41.4 [61]	39.9 [61]	0.601 [61]
AlSb	Experimental	6.1355 [63]	87.7 [63]	43.4 [63]	40.76 [63]	–
	Present	6.1877	86.39	40.65	40.71	0.5893
	Prev. theory	4.460 [64]	293 [56], 252 [19]	159 [56], 129 [19]	155 [56], 147 [19]	0.61 [56]
GaN	Experimental	4.50597 [65], 4.510 [66]	–	–	–	–
	Present	4.4925	288.35	152.98	166.68	0.5678
	Prev theory	5.463 [53], 5.322 [59]	142 [53], 150.7 [61]	61 [53], 62.8 [61]	72 [53], 76.3 [61]	0.516 [61]
GaP	Experimental	5.439 [67]	140 [67]	62 [67]	70 [67]	–
	Present	5.4600	142.16	60.47	72.58	0.5333
	Prev. theory	5.619 [43], 5.75 [19]	125.6 [43], 99 [19]	55.06 [43], 41 [19]	60.56 [43], 51 [19]	0.514 [43]
GaAs	Experimental	5.65325 [68]	113 [68], 120 [67]	57 [68], 53 [67]	60 [68], 60 [67]	0.55 ± 0.02 [69]
	Present	5.6859	116.81	49.64	59.76	0.5288
	Prev. theory	5.981 [59]	92.7 [61]	38.7 [61]	46.2 [61]	0.530 [61]
GaSb	Experimental	6.0959 [63]	88.34 [63]	40.23 [63]	43.22 [63]	–
	Present	6.1524	86.37	36.55	43.44	0.5517
	Prev. theory	4.932 [55]	187 [56], 159 [19]	125 [56], 102 [19]	86 [56], 78 [19]	0.80 [56]
InN	Experimental	4.98 [70], 5.01 [71]	–	–	–	–
	Present	4.9908	185.20	121.72	91.49	0.7474
	Prev. theory	5.899 [53], 5.729 [59]	101 [53], 109.5 [61]	54 [53], 55.7 [61]	48 [53], 52.6 [61]	0.615 [61]
InP	Experimental	5.8687 [63]	101.1 [63]	56.1 [63]	45.6 [63]	–
	Present	5.9035	100.42	53.72	47.39	0.6520
	Prev. theory	6.103 [53], 5.921 [59]	86 [53], 92.2 [61], 72 [18]	45 [53], 46.5 [61], 43 [18]	40 [53], 44.4 [61], 33 [18]	0.598 [61]
InAs	Experimental	6.0583 [63]	83.29 [63]	45.26 [63]	39.59 [63]	–
	Present	6.1160	84.28	44.72	39.66	0.6378
	Prev. theory	6.542 [53], 6.346 [59]	67 [53], 72.0 [61]	34 [53], 35.4 [61]	30 [53], 34.1 [61]	0.603 [61]
InSb	Experimental	6.4794 [63]	69.18 [63]	37.88 [63]	31.32 [63]	0.68 [36]
	Present	6.5625	64.97	33.00	30.42	0.6366

TABLE V. HSE-DFT calculated third-order elastic constants of selected III-V compounds. All calculations have been performed with a cutoff energy of 600 eV, and on a k-point grid density of $10 \times 10 \times 10$. The elastic constants were extracted by fitting to the stresses, the given errors are fitting errors.

	C_{111} (GPa)	C_{112} (GPa)	C_{123} (GPa)	C_{144} (GPa)	C_{155} (GPa)	C_{456} (GPa)
AlN	-1125 ± 3	-1036 ± 8	-44 ± 12	51 ± 3	-789 ± 3	-11.6 ± 0.7
AlP	-595 ± 4	-428 ± 4	-103 ± 6	14.9 ± 0.9	-243 ± 1	-33 ± 1
AlAs	-526 ± 4	-364 ± 3	-86 ± 4	7.1 ± 0.7	-220 ± 1	-27 ± 1
AlSb	-416 ± 3	-268 ± 2	-77 ± 3	6.4 ± 0.5	-156.9 ± 0.6	-21.4 ± 0.7
GaN	-1277 ± 8	-976 ± 4	-252 ± 9	-46 ± 1	-647 ± 2	-49 ± 1
GaP	-753 ± 8	-441 ± 7	-73 ± 7	-10 ± 1	-295 ± 1	-47 ± 1
GaAs	-612 ± 5	-351 ± 4	-86 ± 5	-15.2 ± 0.9	-264 ± 1	-33 ± 1
GaSb	-471 ± 6	-260 ± 5	-63 ± 4	5 ± 1	-192 ± 1	-19.3 ± 0.3
InN	-786 ± 8	-701 ± 8	-327 ± 12	28 ± 2	-290 ± 1	22 ± 1
InP	-491 ± 2.5	-336 ± 2	-131 ± 3.5	-5.17 ± 0.59	-168.6 ± 0.6	-13.6 ± 0.6
InAs	-406 ± 16	-262 ± 15	-132 ± 13	-8.8 ± 0.6	-156 ± 1	-7.9 ± 0.7
InSb	-360 ± 4	-235 ± 3	-94 ± 3	-14 ± 2	-122 ± 1	-6.8 ± 0.8

TABLE VI. Previous experimental and theoretical determinations of third-order elastic constants of GaAs and the cubic III-nitride materials. Theoretical values are italicized.

	C_{111} (GPa)	C_{112} (GPa)	C_{123} (GPa)	C_{144} (GPa)	C_{155} (GPa)	C_{456} (GPa)
AlN	-1070[a]	-965[a]	-61[a]	57[a]	-757[a]	-9[a]
GaN	-1213[a]	-867[a]	-253[a]	-46[a]	-606[a]	-49[a]
GaP	-676 ± 52[b,c]	-499 ± 25[b,c]	-82 ± 56[b,c]	75 ± 47[b,c]	-332 ± 23[b,c]	199 ± 66[b,c]
GaAs	-561[a],-618 ± 9[b,d,e]	-318[a],-389 ± 4[b,d,e]	-70[a],-48 ± 11[b,d,e]	-16[a],50 ± 25[b,d,e]	-242[a],-268 ± 3[b,d,e]	-22[a],-37 ± 10[b,d,e]
GaSb	-475 ± 6[f]	-308 ± 2[f]	-44 ± 29[f]	5 ± 1[f]	-216 ± 13[f]	-25 ± 15[f]
InN	-756[a]	-636[a]	-310[a]	13[a]	-271[a]	15[a]
InAs	-404[g]	-268[g]	-121[a]	-5[g]	-138[g]	-6[g]
InSb	-338 ± 30[b,h]	-242 ± 17[b,h]	-79 ± 14[b,h]	13 ± 7[b,h]	-131 ± 7[b,h]	0 ± 3[b,h]

[a]Reference [19].
[b]Reference [35].
[c]Reference [73].
[d]Reference [74].
[e]Reference [75].
[f]Reference [76].
[g]Reference [18].
[h]Reference [77].

In Table VI, experimental and theoretical values are provided for those materials for which they are available, with theoretical values italicised. We find good agreement between the experimental measurements and our calculated values, taking into account that these measurements are performed often at room temperature ($T \approx 300$ K) where materials tend to be softer [19] than at the $T = 0$ K temperature at which DFT calculations are made. With regard to literature theoretical calculations, for GaAs, there were several different works calculating TOECs [18,19,40,43]. Here, we present only the most contemporary study, by Łopuszyński and Majewski [19]. Overall, we find very good agreement between our results and those obtained via experiment or theory in the literature. This serves as a validation for the extracted constants for which previous experimental or theoretical values are not available.

With the TOECs and SOECs thus determined and validated against previous experimental and theoretical values, we may use them to address the question of when third-order effects become important in the materials under consideration. As a test case, we consider an InSb system that is strained in the x-y plane and free to relax in the z direction. In Fig. 6, the Cauchy stress, σ, in the z direction, of this system is shown. This stress will be relevant to the pressure tuning of the Poisson ratio, and through this the pressure coefficient of the band gap. The figure plots the Cauchy stress, determined three different ways, against the strain. The stress obtained from DFT is given by the symbols, that obtained by linear strain theory is given by the thin green line, and that obtained through third-order finite strain theory is given by the solid red line. Figure 6 shows clearly the increasing failure of the linear theory with increasing strain. By $\pm 5\%$ strain, the linear theory suffers from errors in σ of 26% for -5% strain, and 45% for $+5\%$ strain. This failing of the linear theory at these strains would introduce inaccuracies in the modeling of, for example, the elasticity of InSb/GaSb quantum wells [78] and QDs [23] grown by the Stransky-Krastanov method, given that the lattice mismatch between InSb and GaSb is 6.3%.

Extending this analysis to the other materials, in Fig. 7, the error in the out of plane stress induced by a biaxial strain as calculated by the linear strain theory when compared with the nonlinear theory is plotted as a function of applied strain. From the figure we may infer that once the strain in the system is greater than 2%, the linear theory is no longer appropriate, with the errors in the stress being $\geqslant 10\%$ for all materials, except for AlN, which has a 9% error in the calculated stress at -2% strain. These large nonlinearities in the out of plane stress will manifest most noticeably in the pressure dependent behavior of these materials in their respective heterostructures. Indeed, this has been already demonstrated by Lepkowski [18]. From our results we infer that the pressure tuning of strains in InSb/GaSb structures will be even more
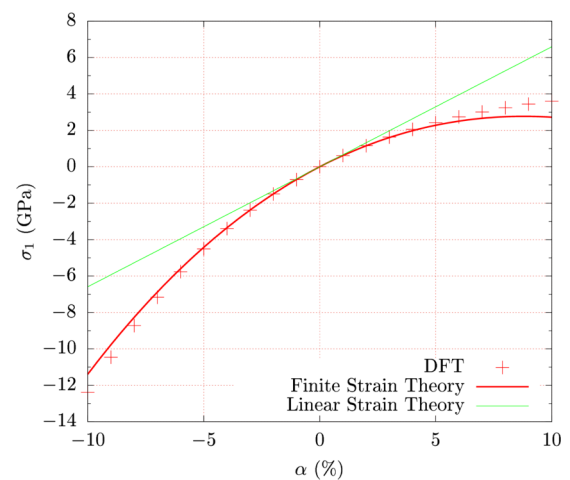

FIG. 6. Nonlinear behavior of $\sigma_1^{(4)}$ for InSb. Red crosses represent HSE-DFT data, whilst the red line shows the nonlinear behavior predicted from Eqs. (20) when C_{ij} and C_{ijk} are fitted on data sets out to $\pm 2\%$ strain; the green line shows the behavior at high strain predicted by linear infinitesimal strain theory. This is the stress that would be obtained in a biaxially strained system, strained equally along y and z axes.

TABLE VII. Internal strain tensor components extracted from HSE-DFT data for Ga, In, and Al containing III-V compounds. Errors given are those associated with least squares fitting.

	A_{14} (Å)	A_{114} (Å)	A_{124} (Å)	A_{156} (Å)
AlN	-0.5888 ± 0.0002	4.339 ± 0.008	4.478 ± 0.009	2.33 ± 0.03
AlP	-0.7936 ± 0.0003	4.01 ± 0.01	5.32 ± 0.01	1.81 ± 0.06
AlAs	-0.8187 ± 0.0003	3.959 ± 0.009	5.385 ± 0.007	1.95 ± 0.06
AlSb	-0.9129 ± 0.0003	3.95 ± 0.01	5.53 ± 0.01	1.72 ± 0.06
GaN	-0.6394 ± 0.0002	4.04 ± 0.02	6.11 ± 0.02	1.97 ± 0.02
GaP	-0.7295 ± 0.0002	3.417 ± 0.008	5.65 ± 0.01	1.98 ± 0.04
GaAs	-0.7533 ± 0.0005	3.584 ± 0.009	5.55 ± 0.01	2.38 ± 0.08
InN	-0.9357 ± 0.0002	5.12 ± 0.05	6.61 ± 0.04	1.23 ± 0.03
InP	-0.9645 ± 0.0004	3.86 ± 0.03	6.72 ± 0.03	1.44 ± 0.07
InAs	-0.9777 ± 0.0004	3.91 ± 0.05	6.58 ± 0.07	1.70 ± 0.06
InSb	-1.0427 ± 0.0009	3.19 ± 0.25	6.61 ± 0.07	1.8 ± 0.1
GaSb	-0.8499 ± 0.0002	3.48 ± 0.02	5.38 ± 0.01	2.20 ± 0.03

markedly nonlinear than that which has already been observed in InAs/GaAs and InN/GaN systems. In the next section, we turn to higher-order effects in the internal strain.

B. Internal strain tensor components

The components of the internal strain tensor are derived from Eqs. (16) and (18). These are given for the strain branches, $\boldsymbol{\eta}^{(1)}$, $\boldsymbol{\eta}^{(2)}$, and $\boldsymbol{\eta}^{(3)}$, in Eq. (22) below:

$$\xi_1^{(1)} = \tfrac{1}{4}(A_{14} + 2A_{156})\beta^2 + A_{14}\beta,$$

$$\xi_1^{(2)} = A_{14}\beta + \tfrac{1}{2}A_{114}\alpha\beta,$$

$$\xi_1^{(3)} = \tfrac{1}{2}(A_{14} + A_{124})\alpha\beta + A_{14}\beta. \tag{22}$$

The extracted nonzero components of the internal strain tensor are given in Table VII. For A_{14}, the values from strain branches $\boldsymbol{\eta}^{(1)}$, $\boldsymbol{\eta}^{(2)}$ and $\boldsymbol{\eta}^{(3)}$, obtained from fitting to Eq. (22) are averaged. Since there is not the same abundance of equations from the relaxed atomic positions to describe

the higher-order internal strain tensor components as there are from the stresses for the elastic constants, the values for the different A_{iJK} are set simply to those of the single independent determination of lowest error. For A_{114}, the only independent determination is that from $\boldsymbol{\eta}^{(2)}$; for A_{156}, it is $\boldsymbol{\eta}^{(1)}$. For A_{124}, there are two independent determinations, but we include in the table only the value from the uncomplicated $\boldsymbol{\eta}^{(3)}$ strain branch.

In terms of comparison with previous calculation or measurement, Table IV reveals very good agreement between our calculated first-order ISTC (the Kleinman parameter) and literature values. To the best of our knowledge, the only other first-principles calculation of the components of the second-order internal strain tensor, are given only for C, in Ref. [42]. However, strain derivatives of the Kleinman parameter are available for Si in Ref. [40], and for GaAs in Ref. [25]. While these strain derivatives for the case of GaAs could be related to our data in Table VII, we find that the obtained Kleinman parameter of Ref. [25], 0.455, disagrees significantly with our obtained value, 0.5288, with those from experiment, 0.55 ± 0.02 [69], and with those from more recent theory 0.514 [43], 0.517 [79]; we do not therefore attempt explicit comparison.

V. CONCLUSION

In summary, second- and third-order elastic and first- and second-order internal strain tensor components were extracted from accurate HSE DFT calculations. The elastic constants and internal strain tensor components were extracted via stress-strain and position-strain relations expressed within the formalism of finite strain, respectively. This is the first determination of many of these constants. In particular, the components of the second-order internal strain tensor extracted here have not before been measured or calculated. Where previously determined, good agreement was obtained with experiment and theory found in the literature. The results of convergence checks presented illustrate that far greater care must be taken in the determination of third-order elastic constants (TOECs) as compared to second-order elastic constants (SOECs), with a high resolution of calculation required. The use of the stress-strain equations for the
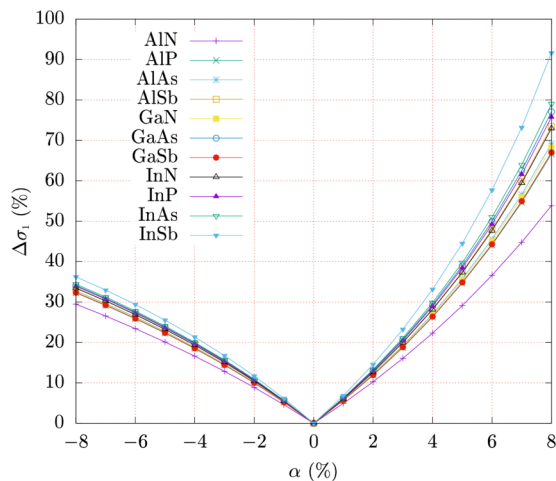

FIG. 7. Percentage error in $\sigma_1^{(4)}$, $\Delta\sigma = \frac{\sigma_{\text{nonlin}} - \sigma_{\text{lin}}}{\sigma_{\text{nonlin}}}$, where the error is the difference between the stress as predicted using third-order finite strain theory σ_{nonlin} and that predicted using a second-order infinitesimal strain theory σ_{lin} as a function of increasing strain α.

calculation of elastic constants was justified, and arguments from the literature, formulated in the context of SOECs, were shown to have even more force in the case of third-order elastic constants. The impact of nonlinear strain effects was demonstrated in particular for the elasticity of InSb, and in general for other III-V materials systems, where it was found that third-order effects become significant for as little as 2% strain. Knowledge of the elastic constants and internal strain tensor components presented here should therefore prove useful for the modeling of highly mismatched III-V heterostructures.

[1] E. P. O'Reilly, Semicond. Sci. Technol. **4**, 121 (1989).

[2] J. F. Nye, *Physical Properties of Crystals: Their Representation by Tensors and Matrices*, 2nd ed. (Oxford University Press, Oxford, 1985).

[3] M. A. Moram and M. E. Vickers, Rep. Prog. Phys. **72**, 036502 (2009).

[4] D. Holec, P. Costa, M. Kappers, and C. Humphreys, J. Cryst. Growth **303**, 314 (2007), proceedings of the Fifth Workshop on Modeling in Crystal Growth.

[5] C. Kittel, *Introduction to Solid State Physics*, 8th ed. (Wiley, New York, 2004).

[6] O. Brand, I. Dufour, S. M. Heinrich, and F. Josse, *Resonant MEMS: Fundamentals, Implementation and Application* (Wiley-VCH, Weinheim, 2015).

[7] P. N. Keating, Phys. Rev. **145**, 637 (1966).

[8] M. Born and K. Huang, *Dynamical Theory of Crystal Lattices*, Oxford Classic Texts in the Physical Sciences (Clarendon Press, Oxford, 1954).

[9] L. Kleinman, Phys. Rev. **128**, 2614 (1962).

[10] C. S. G. Cousins, J. Phys. C: Solid State Phys. **11**, 4867 (1978).

[11] J. L. Birman, Phys. Rev. **111**, 1510 (1958).

[12] R. M. Martin, Phys. Rev. B **5**, 1607 (1972).

[13] L. Landau and E. Lifshitz, *Theory of Elasticity*, 3rd ed. (Butterworth-Heinemann, Kidlington, Oxford, 1986).

[14] C. Pryor, J. Kim, L. W. Wang, A. J. Williamson, and A. Zunger, J. Appl. Phys. **83**, 2548 (1998).

[15] M. D. Frogley, J. R. Downes, and D. J. Dunstan, Phys. Rev. B **62**, 13612 (2000).

[16] S. W. Ellaway and D. A. Faux, J. Appl. Phys. **92**, 3027 (2002).

[17] B. S. Ma, X. D. Wang, F. H. Su, Z. L. Fang, K. Ding, Z. C. Niu, and G. H. Li, J. Appl. Phys. **95**, 933 (2004).

[18] S. P. Łepkowski, Phys. Rev. B **78**, 153307 (2008).

[19] M. Łopuszyński and J. A. Majewski, Phys. Rev. B **76**, 045202 (2007).

[20] S. Łepkowski and J. Majewski, Solid State Commun. **131**, 763 (2004).

[21] S. P. Łepkowski, J. A. Majewski, and G. Jurczak, Phys. Rev. B **72**, 245201 (2005).

[22] W. Shan, J. W. Ager, W. Walukiewicz, E. E. Haller, M. D. McCluskey, N. M. Johnson, and D. P. Bour, Phys. Rev. B **58**, R10191 (1998).

[23] N. Deguffroy, V. Tasco, A. N. Baranov, E. Tournié, B. Satpati, A. Trampert, M. S. Dunaevskii, A. Titkov, and M. Ramonda, J. Appl. Phys. **101**, 124309 (2007).

[24] M. A. Caro, S. Schulz, and E. P. O'Reilly, Phys. Rev. B **91**, 075203 (2015).

[25] M. A. Migliorato, D. Powell, A. G. Cullis, T. Hammerschmidt, and G. P. Srivastava, Phys. Rev. B **74**, 245332 (2006).

[26] Y. Hiki, Annu. Rev. Mater. Sci. **11**, 51 (1981).

[27] C. S. G. Cousins, Ph.D. thesis, University of Exeter, 2001.

[28] K. Brugger, Phys. Rev. **133**, A1611 (1964).

[29] P. N. Keating, Phys. Rev. **149**, 674 (1966).

[30] F. Birch, Phys. Rev. **71**, 809 (1947).

[31] D. C. Wallace, *Solid State Physics*, edited by H. Ehrenreich, F. Seitz, and D. Turnbull, Vol 25 (Academic Press, New York, 1970), pp. 301–404.

[32] R. N. Thurston and K. Brugger, Phys. Rev. **133**, A1604 (1964).

[33] F. D. Murnaghan, *Finite Deformation of an Elastic Solid* (Wiley, London, 1951).

[34] F. D. Murnaghan, Am. J. Math. **59**, 235 (1937).

[35] A. S. Johal and D. J. Dunstan, Phys. Rev. B **73**, 024106 (2006).

[36] C. S. G. Cousins, L. Gerward, J. S. Olsen, S. A. Sethi, and B. J. Sheldon, Phys. Status Solidi A **126**, 135 (1991).

[37] J. M. Lang and Y. M. Gupta, Phys. Rev. Lett. **106**, 125502 (2011).

[38] K. S. Chandrasekaran, S. K. Mohanlal, and R. Saravanan, Phys. Status Solidi B **196**, 3 (1996).

[39] T. Suzuki, A. V. Granato, and J. F. Thomas, Phys. Rev. **175**, 766 (1968).

[40] O. H. Nielsen and R. M. Martin, Phys. Rev. B **32**, 3792 (1985).

[41] A. Hmiel, J. M. Winey, Y. M. Gupta, and M. P. Desjarlais, Phys. Rev. B **93**, 174113 (2016).

[42] O. H. Nielsen, Phys. Rev. B **34**, 5808 (1986).

[43] J. Sörgel and U. Scherz, Eur. Phys. J. B **5**, 45 (1998).

[44] J. Heyd, G. E. Scuseria, and M. Ernzerhof, J. Chem. Phys. **118**, 8207 (2003).

[45] W. Voigt, *Lehrbuch der Kristallphysik* (Teubner, Leipzig, 1928).

[46] O. H. Nielsen and R. M. Martin, Phys. Rev. Lett. **50**, 697 (1983).

[47] C. S. G. Cousins, J. Phys. C: Solid State Phys. **11**, 4881 (1978).

[48] M. A. Caro, S. Schulz, and E. P. O'Reilly, J. Phys.: Condens. Matter **25**, 025803 (2013).

[49] D. S. P. Tanner, Ph.D. thesis, University College Cork, 2017.

[50] G. Kresse and J. Furthmüller, Phys. Rev. B **54**, 11169 (1996).

[51] T. M. Henderson, J. Paier, and G. E. Scuseria, Phys. Status Solidi B **248**, 767 (2011).

[52] J. Paier, M. Marsman, K. Hummer, G. Kresse, I. C. Gerber, and J. G. Ángyán, J. Chem. Phys. **124**, 154709 (2006).

[53] M. Råsander and M. A. Moram, J. Chem. Phys. **143**, 144104 (2015).

[54] R. Golesorkhtabar, P. Pavone, J. Spitaler, P. Puschnig, and C. Draxl, Comput. Phys. Commun. **184**, 1861 (2013).

[55] A. F. Wright and J. S. Nelson, Phys. Rev. B **51**, 7866 (1995).

[56] A. F. Wright, J. Appl. Phys. **82**, 2833 (1997).

[57] D. J. As, Proc. SPIE **7608**, 76080G (2010).

[58] I. Petrov, E. Mojab, R. C. Powell, J. E. Greene, L. Hultman, and J. Sundgren, Appl. Phys. Lett. **60**, 2491 (1992).

[59] S. Q. Wang and H. Q. Ye, Phys. Rev. B **66**, 235111 (2002).

[60] Physics of semiconductors and their heterostructures in *Physics of Semiconductors and Their Heterostructures*, edited by J. Singh (McGraw-Hill, New York, 1993).

[61] S. Q. Wang and H. Q. Ye, Phys. Status Solidi B **240**, 45.

[62] V. Bessolov, S. Konnikov, and V. Umanskii, Fiz. Tverd. Tela **24**, 1528 (1982).

[63] *Semiconductors: Data Handbook,* edited by O. Madelung, 3rd ed. (Springer-Verlag GmbH, Berlin, Heidelberg, 2003).

[64] A. F. Wright and J. S. Nelson, Phys. Rev. B **50**, 2159 (1994).

[65] M. Frentrup, L. Y. Lee, S.-L. Sahonta, M. J. Kappers, F. Massabuau, P. Gupta, R. A. Oliver, C. J. Humphreys, and D. J. Wallis, J. Phys. D: Appl. Phys. **50**, 433002 (2017).

[66] S. V. Novikov, N. Zainal, A. V. Akimov, C. R. Staddon, A. J. Kent, and C. T. Foxon, J. Vac. Sci. Technol. B **28**, C3B1 (2010).

[67] *Springer Materials*, edited by O. Madelung, U. Rössler, and M. Schulz (Springer-Verlag GmbH, Berlin, Heidelberg, 1998), pp. 1–9.

[68] J. S. Blakemore, J. Appl. Phys. **53**, R123 (1982).

[69] C. S. G. Cousins, L. Gerward, J. S. Olsen, B. Selsmark, B. J. Sheldon, and G. E. Webster, Semicond. Sci. Technol. **4**, 333 (1989).

[70] S. Strite, D. Chandrasekhar, D. J. Smith, J. Sariel, H. Chen, N. Teraguchi, and H. Morkoç, J. Cryst. Growth **127**, 204 (1993).

[71] J. Schörmann, D. J. As, K. Lischka, P. Schley, R. Goldhahn, S. F. Li, W. Löffler, M. Hetterich, and H. Kalt, Appl. Phys. Lett. **89**, 261903 (2006).

[72] J. P. Perdew, K. Burke, and M. Ernzerhof, Phys. Rev. Lett. **77**, 3865 (1996).

[73] Y. Yoḡurtçu, A. Miller, and G. Saunders, J. Phys. Chem. Solids **42**, 49 (1981).

[74] J. R. Drabble and A. J. Brammer, Proc. Phys. Soc. **91**, 959 (1967).

[75] H. J. McSkimin and P. Andreatch, Jr., J. Appl. Phys. **38**, 2610 (1967).

[76] V. S. Raja and P. J. Reddy, Phys. Lett. A **56**, 215 (1976).

[77] V. Raja and P. Reddy, Solid State Commun. **21**, 701 (1977).

[78] L. Q. Qian and B. W. Wessels, Appl. Phys. Lett. **63**, 628 (1993).

[79] J. E. Raynolds, Z. H. Levine, and J. W. Wilkins, Phys. Rev. B **51**, 10477 (1995).